Electronic Supplementary Material (ESI) for Nanoscale.

Supporting Information

A bioinspired solar evaporator with horizontal channel-like framework for efficient and stable high-salinity brine desalination

Shuqian Zhang,[a] Han Wei,[b] Zhijian Zhang,[c] Jianzhong Zhang,[c] Hua Bao,[b] Wang Zhang*[a]

Supplementary Notes

Note S1. Emissivity calculation

The emissivity is an intrinsic property of the material. The emissivity (ε) is the ratio of the total emissive power of a real surface to that of a blackbody at the same temperature. The emissivity is calculated with the following equation[1]

$$\varepsilon = \frac{\int_{2.5\,\mu m}^{25\,\mu m} [1 - R(\lambda)] P_B(\lambda) d\lambda}{\int_{2.5\,\mu m}^{25\,\mu m} P_B(\lambda) d\lambda} \quad \text{(S1)}$$

where the denominator and the numerator are the total emissivity power of a blackbody and the total energy emitted by the materials in the wavelength range from 2.5 to 25 μm, respectively. *R(λ)* is the reflection measured in the wavelength range, $P_B(\lambda)$ is the spectral radiance of a blackbody at the measured temperature, given by Plank's law. The figure below shows the reflectance spectra of CEP in the range of 2.5 to 25 μm. According to the equation (S1), the emissivity (ε) of the carbonized eggplant is calculated to be 0.95.

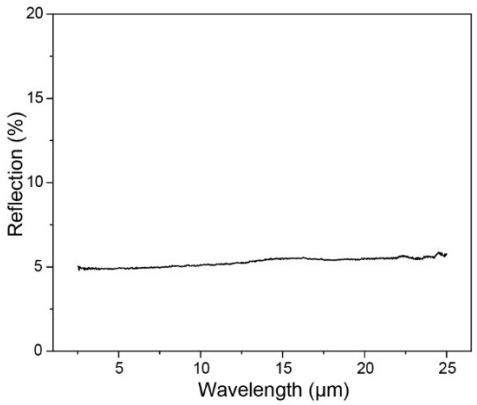

Infrared reflection spectra of CEP.

Note S2. Optical absorption calculation

Optical measurements were carried out with a UV–vis Spectrometer Lambda 35 from 250 to 2500 nm (PerkinElmer, USA) that equipped with an integrated sphere. The absorbance (*A*) measurement

was calculated based on transmittance (T) and reflectance (R) measurement (A=1-R-T), where R and T are the reflection and transmission of the samples, respectively. The absorption values of different samples were calculated based on the Equation S2:

$$\alpha = \frac{\int_{280}^{2500} I(\lambda)A(\lambda)d\lambda}{\int_{280}^{2500} I(\lambda)d\lambda} \quad \text{(S2)}$$

Note S3. Test of thermal conductivity

The thermal conductivities perpendicular and parallel to the fiber growth direction of CEP are measured and calculated using the Equation S3,

$$k = \rho\alpha c \quad \text{(S3)}$$

where ρ is the volumetric mass density, which was calculated from the weight and volume; a is the thermal diffusivity perpendicular and parallel to the fiber growth direction, which was measured with a Netzsch LFA 447 Nano flash equipment, and c is the specific heat capacity, which was measured using a differential scanning calorimetry (DSC) equipment (Perkin Elmer DSC8000). During the measurement, the thermal conductivities perpendicular and parallel to the fiber growth direction are tested with sample CEP-H and CEP-V, respectively. The sample size is 1 cm × 1 cm, thickness t <1 mm. The thermal conductivity result is shown in Table S1.

Note S4. Water evaporation efficiency (η)

The evaporation rate was calculated according to the linear fitting result from the mass change curves of water with time. The evaporation efficiencies were calculated based on the Equation S4:

$$\eta = \frac{mh_{LV}}{C_{opt}P_0} \quad \text{(S4)}$$

where m is the water evaporation rate subtracted by the value in dark area ($m = m_{light} - m_{dark}$, m_{dark} = 0.11 kg m^{-2} h^{-1} in this study), P_0 is the nominal solar irradiation value of 1 kW m^{-2}, C_{opt}

represents the optical concentration, h_{LV} is the total enthalpy of liquid-steam phase change. h_{LV} includes the sensible heat of water and the phase-change enthalpy and can be calculated using the Equation S5:

$$h_{LV} = c\Delta T + \Delta h \tag{S5}$$

where is c the specific heat capacity of water (4.2 kJ kg^{-1} K^{-1}), ΔT is the temperature increase of water from 25 ℃ to ~37.7 ℃ as shown in Fig. S6, and the Δh is the phase-change enthalpy at the temperature of evaporation surface (2410 kJ kg^{-1} at ~38 ℃). Thus, h_{LV} is calculated to be 2465 kJ kg^{-1}. The efficiencies under different sun irradiation were calculated in the same way. The temperatures and h_{LV} under different sun irradiation were shown in Fig. S9 and Table S3.

Note S5. Heat loss analysis

The heat loss of the solar evaporator through three forms: (1) radiation (2) convection and (3) conduction. The details of analysis are shown below.

Radiation:

The radiation loss was calculated by Stefan-Boltzman equation:

$$\phi = \varepsilon A\sigma(T_1^4 - T_2^4) \tag{S6}$$

where ϕ represents the heat flux, ε is the emissivity (~0.95), A denotes the evaporation surface area (4.9 cm^2), σ is the Stefan-Boltzman constant (5.67×10^{-8} W m^{-2} K^{-4}), T_1 is the average temperature of evaporation surface (~ 37.7 ℃) at a steady condition, T_2 is the ambient temperature (~34.9 ℃) above the absorber as shown in Fig. S7. According to the Equation S6, the radiation heat loss is calculated to be ~1.9 % under one sun illumination.

Convection:

The convection loss was calculated by Newton's law of cooling:

$$Q = hA\Delta T \tag{S7}$$

where Q represents the heat, h is the convection heat transfer coefficient (5 W m^{-2} K^{-1}), A is the surface area (4.9 cm^2), ΔT denotes the difference between the surface temperature and ambient temperature above the absorber. Based on the Equation S5, the convection heat loss is 1.5%.

Conduction:

The conduction heat loss is the heat transferred directly from the absorber to the bulk water.

$$Q = cm\Delta T \tag{S8}$$

where Q denotes the heat, c is the specific heat capacity of water (4.2 kJ kg^{-1} K^{-1}), m represents the weight of bulk water 50 g, ΔT is the increased temperature of bulk water caused by heat transferred from the absorber. In this work, temperature of bulk water increases 2.5 K without absorber. When the absorber is CEP-H, temperature of bulk water increases 2.7 K. Thus, the ΔT =0.2 K. The conduction heat loss from CEP-H is calculated to account for 2.4% of total energy. Based on the analysis above, the total heat loss is ~5.8% and the rest energy was used for reflection (3.5%), water evaporation (~ 90.6%) and other dissipation. Likewise, the energy loss of CEP-V can be analyzed. The light absorbing loss, radiative loss and convective loss of for CEP-V are similar to CEP-H. In comparison, the conduction heat loss from CEP-V is calculated to account for 9.7% of total energy, which is agreed with the calculated evaporation efficiency of 80.9%.

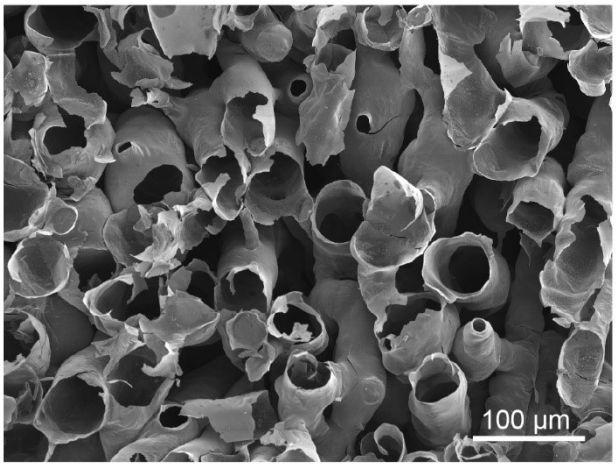

Fig. S1. Side view scanning electron microscopy (SEM) images of eggplant.

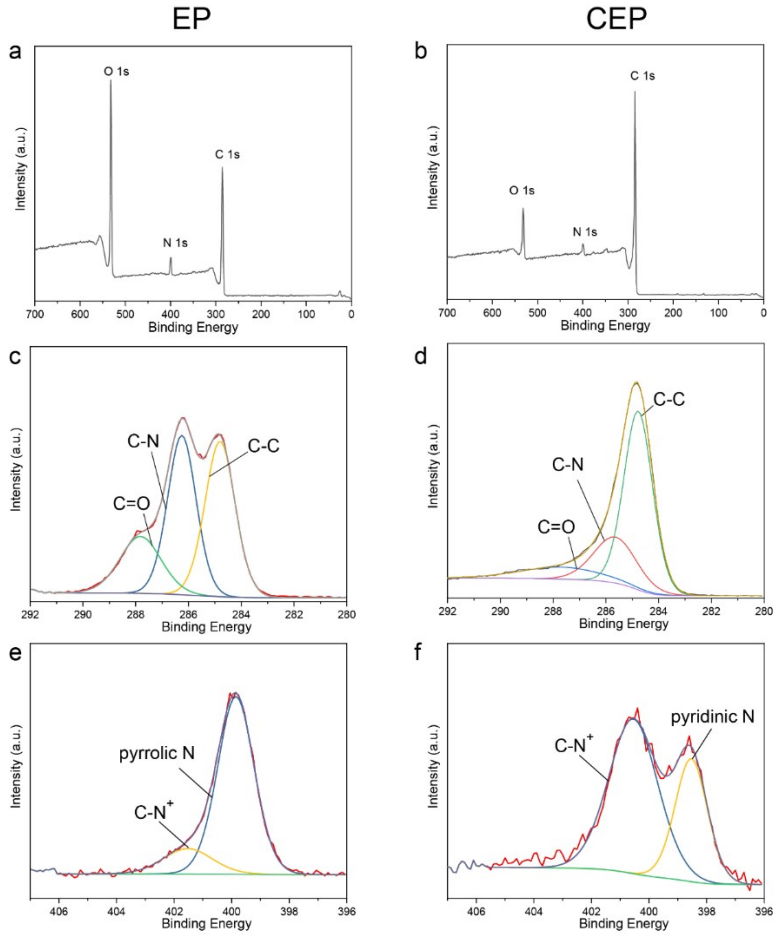

Fig. S2. XPS spectra of EP and CEP. XPS full scan spectra of (a) EP, (b) CEP. (c) High-resolution N 1s spectra of EP. (d) High-resolution N 1s spectra of CEP. (e) High-resolution N 1s spectra of

EP. (f) High-resolution N 1s spectra of CEP.

The XPS survey spectrums of the EP and CEP present three main elements including carbon element, oxygen element, and nitrogen element in both EP and CEP. The high-resolution C 1s spectra of EP and CEP show that the C–C bond dominated after pyrolysis and endowed CEP with efficient absorption throughout the whole solar spectrum. The high-resolution C 1s spectra of CEP are deconvoluted to three different peaks at 284.7, 285.6, and 287.7 eV, corresponding to C-C/C=C, C-N, and C=O, respectively. Additionally, as shown in the N 1s spectra, the characteristic peak around 399.86 eV, which is corresponding to C-N, proves the existence of hydrophilic nitrogenous functional groups.

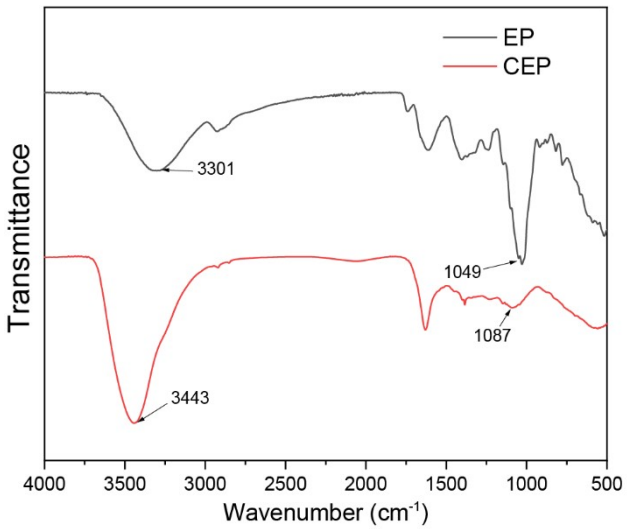

Fig. S3. FTIR spectra of EP and CEP.

In the FTIR spectra of CEP, the peaks at 1087 cm^{-1} and 3443 cm^{-1} confirm the existence of hydrophilic group C-N/N-H. The signal intensities of oxygen-containing groups decrease, indicating the oxidation occurs during the carbonization process. The surface of the CEP is highly hydrophilic due to the functional groups and elementary composition, which is beneficial for

efficient water absorption and transportation.

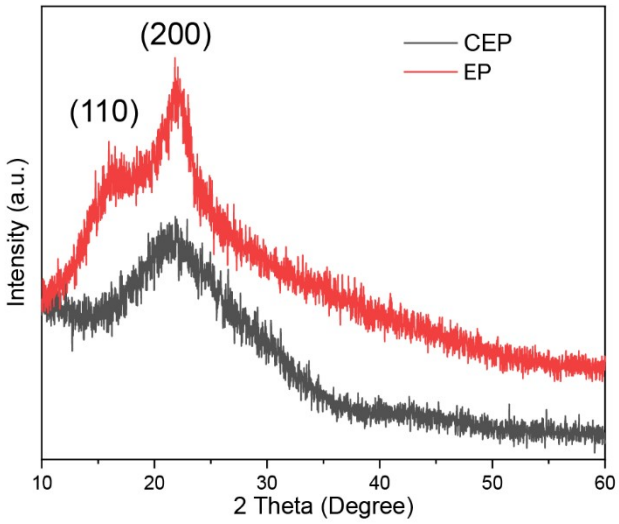

Fig. S4. XRD spectra of EP and CEP.

According to the XRD pattern of EP and CEP, they are predominantly composed of cellulose and amorphous carbon, respectively. The diffraction peaks are attributed to the (110) and (200) plane of cellulose. The broad diffraction peaks appear reveal the low crystalline of CEP.

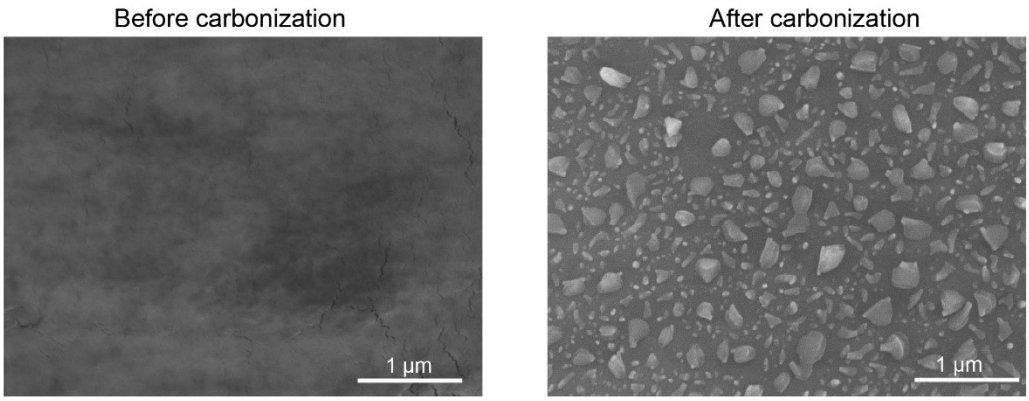

Fig. S5. Surface morphology of EP and CEP.

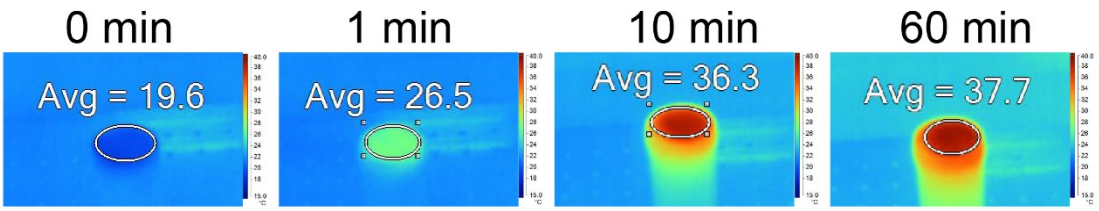

Fig. S6. Infrared thermal images of the CEP-H during the solar evaporation for 1 h under one sun irradiation.

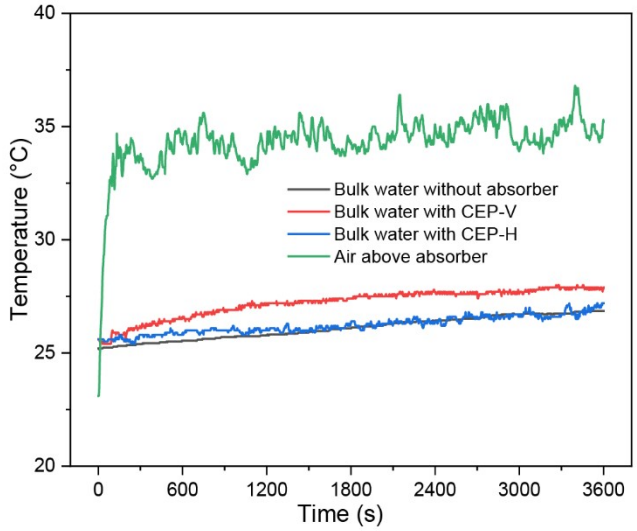

Fig. S7. The temperature of air above absorber, and the temperature of the bulk water without absorber and with CEP-H, CEP-V as absorber under one sun illumination.

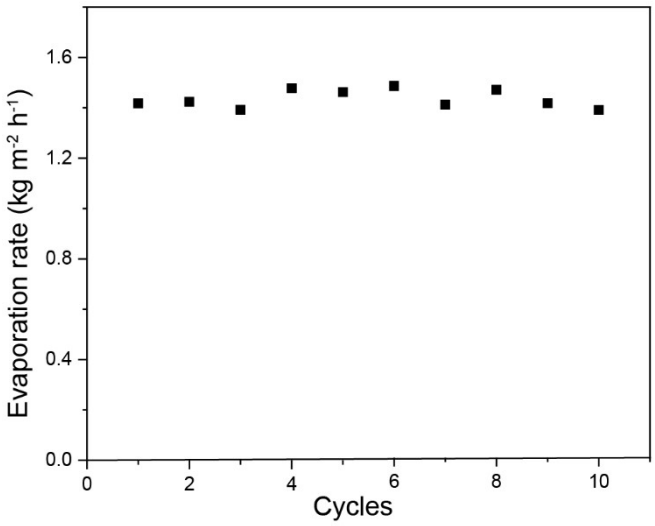

Fig. S8. Cycle test of CEP-H treating pure water for 1 h under one sun irradiation.

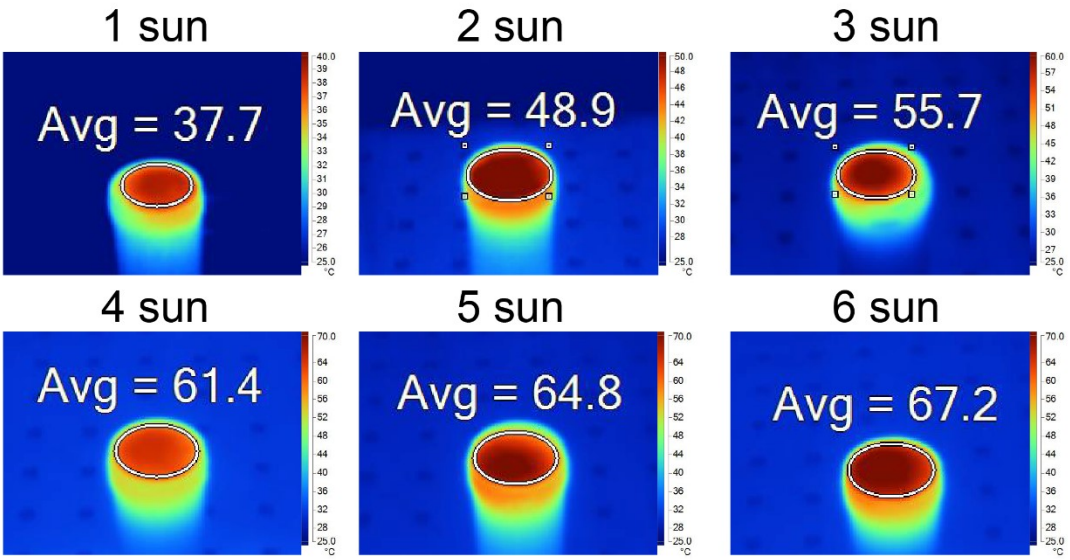

Fig. S9. Infrared thermal images of the CEP-H during the solar evaporation for 1 h under different sun irradiation.

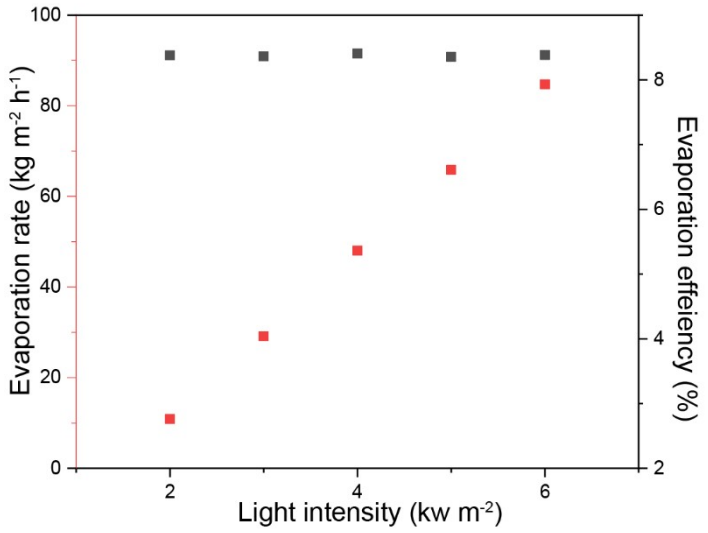

Fig. S10. Evaporation rates and efficiencies of CEP-H under the light intensity of 2-6 kW m^{-2}.

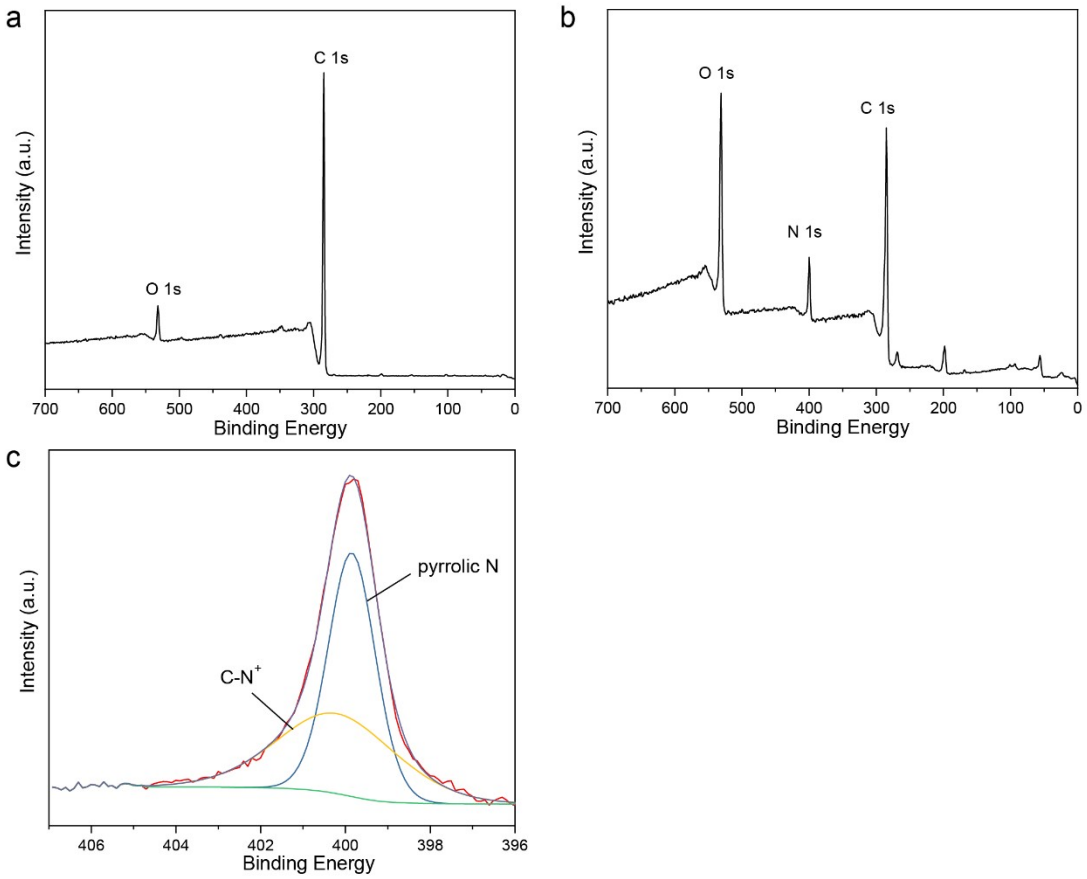

Fig. S11. XPS spectra of pristine PP and PPy/PP. XPS full scan spectra of (a) pristine PP, (b) PPy/PP. (c) High-resolution N 1s spectra of PPy/PP.

X-ray photoelectron spectroscopy (XPS) was performed to investigate the elemental composition of PP and PPy/PP. Apart from the obvious signal of O and C elements in pristine PP, N (10.78 at%) can be found in the sample after PPy coating. The high-resolution XPS spectrum of N 1s can be deconvoluted into pyrrolic N (399.8 eV) and C-N^+(400.4 eV).

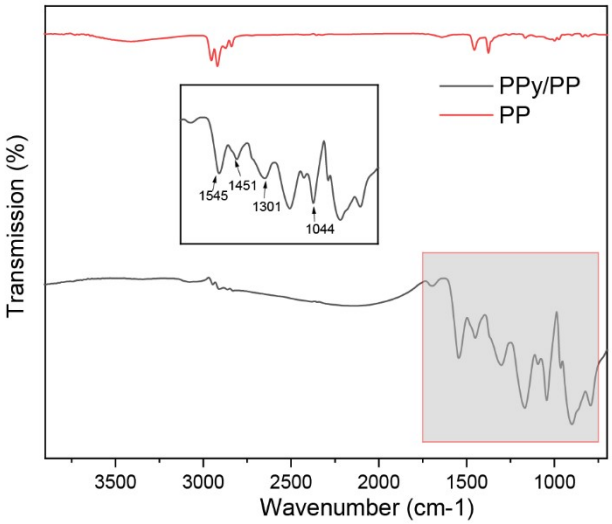

Fig. S12. FTIR spectra of pristine PP and PPy/PP. The inset is the partial enlarged view of PPy/PP, indicating the characteristic peaks.

The characteristic peaks of 1545, 1451, 1301 and 1044 cm^{-1} in FTIR spectrum of PPy/PP represent C-C/C=C stretching, vibration of pyrrole ring, C-N stretching vibration, and the in-plane deformation of N–H bonds, respectively, proving the existence of PPy.

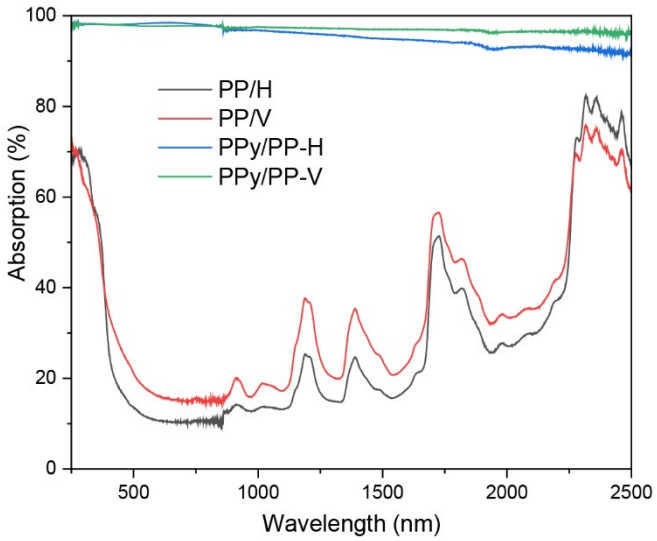

Fig. S13. Solar absorption spectra of PP-H, PP-V, PPy/PP-H, and PPy/PP -V.

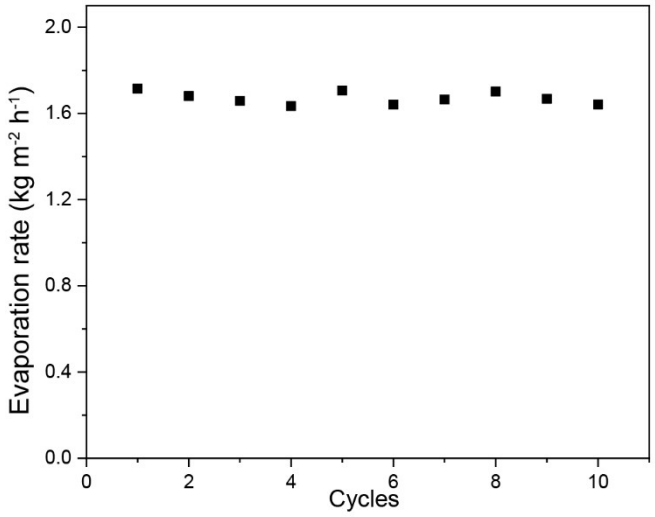

Fig. S14. Cycle test of PPy/PP-H treating pure water for 1 h under one sun irradiation.

Table S1. Thermal conductivity determination for CEP.

Sample	**Density ρ (g cm^{-3})**	**Thermal diffusivity α (mm^2 g^{-1})**	**Specific heat capacity *c* (J g k^{-1})**	**Thermal conductivity k (W m^{-1} K^{-1})**
CEP-V (parallel to the fiber growth direction)	0.0245	1.502±0.018	2.042	0.0751±0.0009
CEP-H (perpendicular to the fiber growth direction)	0.0245	0.846±0.008	2.042	0.0423±0.0004

Table S2. The simulated thermal conductivities for Model 1,2 and 3. The unit is W m^{-1} K^{-1}.

	Model 1	Model 2	Model 3
1	0.028909	0.051086	0.078792
2	0.028970	0.051181	0.082499
3	0.028988	0.053919	0.083956
4	0.028962	0.052441	0.084777
5	0.028973	0.052673	0.077222
Average simulated thermal conductivity	0.02896±0.00003	0.05226±0.00117	0.08145±0.00329

Table S3. The total enthalpy of liquid-steam phase change under different sun illumination.

Light intensity (kw m^{-2})	**1**	**2**	**3**	**4**	**5**	**6**
h_{LV} (kJ kg^{-1})	2465	2480	2497	2508	2512	2517

Reference

1. J. Zhou, Y. Gu, P. Liu, P. Wang, L. Miao, J. Liu, A. Wei, X. Mu, J. Li and J. Zhu, *Adv. Funct. Mater.*, 2019, **29**. 1903255